How to cite: *Angew. Chem. Int. Ed.* **2023,** *62,* e202301356
International Edition: doi.org/10.1002/anie.202301356
German Edition: doi.org/10.1002/ange.202301356

Nanographenes

Heptagon-Containing Nanographene Embedded into [10]Cycloparaphenylene

Juan P. Mora-Fuentes, Marcos D. Codesal, Marco Reale, Carlos M. Cruz, Vicente G. Jiménez, Alice Sciortino, Marco Cannas, Fabrizio Messina, Victor Blanco,* and Araceli G. Campaña**

In memory of Professor J. Enrique Oltra

Abstract: We report the synthesis and characterization of a novel type of nanohoop, consisting of a cycloparaphenylene derivative incorporating a curved heptagon-containing π-extended polycyclic aromatic hydrocarbon (PAH) unit. We demonstrate that this new macrocycle behaves as a supramolecular receptor of curved π-systems such as fullerenes C_{60} and C_{70}, with remarkably large binding constants (ca. $10^7\,M^{-1}$), as estimated by fluorescence measurements. Nanosecond and femtosecond spectroscopic analysis show that these host-guest complexes are capable of quasi-instantaneous charge separation upon photoexcitation, due to the ultrafast charge transfer from the macrocycle to the complexed fullerene. These results demonstrate saddle-shaped PAHs with dibenzocycloheptatrienone motifs as structural components for new macrocycles displaying molecular receptor abilities and versatile photochemical responses with promising electron-donor properties in host-guest complexes.

[*] Dr. J. P. Mora-Fuentes, M. D. Codesal, Dr. C. M. Cruz, Dr. V. G. Jiménez, Dr. V. Blanco, Dr. A. G. Campaña
Departamento de Química Orgánica and Unidad de Excelencia de Química (UEQ), Facultad de Ciencias, Universidad de Granada
Avda. Fuente Nueva s/n, 18071 Granada (Spain)
E-mail: victorblancos@ugr.es
araceligc@ugr.es

M. Reale, Dr. A. Sciortino, Prof. M. Cannas, Prof. F. Messina
Department of Physics and Chemistry (DiFC) "E. Segrè", University of Palermo
90123 Palermo (Italy)
E-mail: fabrizio.messina@unipa.it

Dr. C. M. Cruz
Department of Chemistry, University of Zurich
Winterthurerstrasse 190, 8057 Zurich (Switzerland)

Introduction

Cycloparaphenylenes (CPPs) are a family of radially π-conjugated nanohoops based on benzene rings,[1] which have been extensively studied during the last decade owing to the available and versatile synthetic methodologies.[2] Their applicability ranges from solution and solid-state fluorophores to organic electronic components,[3] including as well bioimaging or size separation.[4] Remarkably, most of these applications arise from the capacity of CPPs to act as supramolecular hosts.[5] Particularly, their supramolecular assemblies with fullerenes are well known and have been widely studied.[6]

On the other hand, π-extended CPPs have received major attention during the last years since they combine the spatial arrangement of CPPs and the electronic properties of polycyclic aromatic hydrocarbons (PAHs).[7,8] These hybrid materials open new pathways for the directed engineering of the properties of pristine CPPs, as done for example by the inclusion of donor, acceptor, or antiaromatic PAHs as part of the CPP structure. [9,10,11] Furthermore, π-extended CPPs are interesting hosts for fullerenes.[12] In such systems, the supramolecular interactions between the CPP and fullerenes, such as C_{60}, can be modulated depending on the PAH nature. For instance, embedding large PAHs, e.g. hexa-*peri*-hexabenzocoronene (HBC), into the CPP structure influences the binding affinity. Thus, the binding constant (K_a) increased by one order of magnitude in HBC-[10]CPP in comparison to parent [10]CPP ($K_a = 2.33\times10^7$ vs $2.79\times10^6\,M^{-1}$).[6a,12d] Yang, Du, Nishiuchi, Müllen, Ito and co-workers have presented a family of HBC-containing CPPs (Figure 1),[12b-e,g,13] some of them with high binding constants with fullerenes and proved that π-extended macrocycles are promising electron donor motifs for the preparation of electroactive devices.[12d]

The study of the supramolecular interactions between fullerenes and curved PAHs other than corannulene-based systems,[14] like contorted, double-concave or heptagon-containing negatively curved nanographenes, has been gaining special attention over the last few years.[15] The curved geometry of these nanographenes induces a shape complementarity with fullerenes that favors their binding. In some cases, charge transfer processes have been described,[15b,c,f] enabling remarkable applications such as in

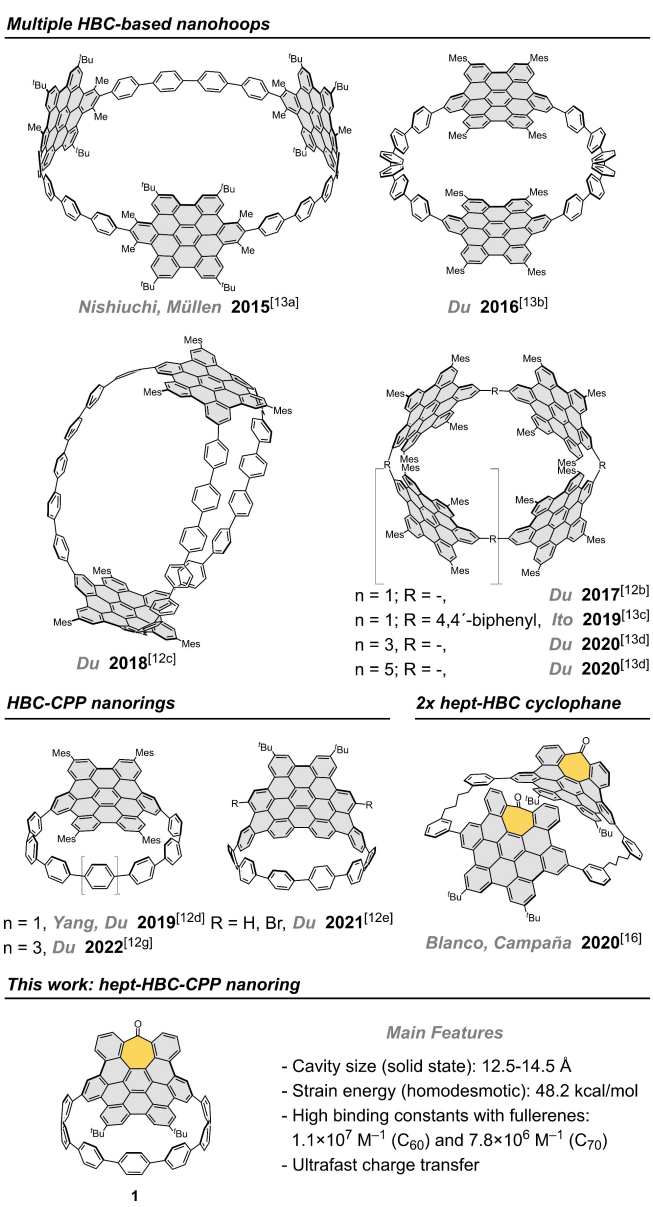

Figure 1. HBC-CPP hybrid nanohoops and *hept*-HBC-based cyclophane previously synthesized and structure of *hept*-HBC [10]CPP **1** presented in this work.

photovoltaics,[15b,c] and potentially in photocatalysis and artificial photosynthesis. Within this line, our research group recently reported a flexible macrocycle based on two heptagon-containing HBCs (*hept*-HBC), linked through flexible alkyl chains (Figure 1).[16] In our previous macrocycle, the shape complementarity of the *hept*-HBCs combined with the flexibility of the structure favored the binding of fullerenes C_{60} and C_{70}, however with selectivity for C_{70}, even in the presence of C_{60}. Nevertheless, the incorporation of heptagon-containing saddle-shaped nanographenes into a CPP scaffold, creating rigid macrocyclic structures, and the study of their behavior as hosts of curved π-systems are still unexplored.

In this paper, we describe the synthesis and characterization of a new type of nanohoop constituted by one unit of saddle-shaped heptagon-containing HBC (*hept*-HBC) embedded within a [10]CPP motif (*hept*-HBC [10]CPP **1**, Figure 1), and we evaluate its capability to act as a fullerene receptor through the establishment of π interactions and the photophysical response of the resulting host-guest complexes.

Results and Discussion

The synthesis of **1** is depicted in Scheme 1 and it is initiated from the previously reported dibromo *hept*-HBC derivative **2**,[17] that can be easily prepared by following our described methodology for the preparation of functionalized *hept*-HBCs.[18] The synthetic route towards **1** follows the strategy developed by Jasti and co-workers, using cyclohexadiene units as *masked* benzene rings and a final reductive aromatization.[19] The key step is the macrocyclization reaction through a Suzuki cross-coupling in dilute conditions between **2** and the diboronate ester of the para-phenylene

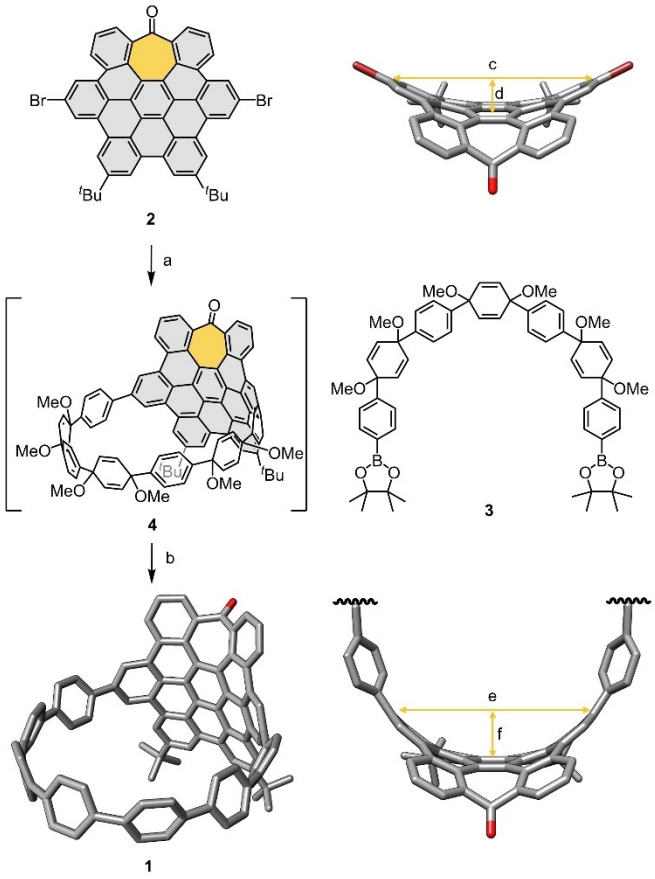

Scheme 1. Synthesis and X-ray structure of **1** and DFT optimized (ωB97XD/def2-SVP) structure of **2**. H atoms have been omitted for clarity. Color coding: C, gray; O, red, Br, dark red. Reagents and conditions: a) **3**, $Pd(PPh_3)_4$, Cs_2CO_3, THF/H_2O, 80 °C, 48 h; b) $SnCl_2$, $HCl_{(c)}$; THF, RT, 52 h, 21% (two steps). Distances [Å]: c) 10.70; d) 1.60; e) 9.75; f) 2.42.

precursor **3** (see Supporting Information for its synthesis). Thus, precursor **4** was obtained and directly subjected to the final reduction step promoted by a mixture of $SnCl_2$ and $HCl_{(c)}$, satisfactorily yielding the *hept*-HBC-containing [10]CPP **1** in 21 % yield (over two steps). It should be pointed that *hept*-HBC derivatives show an intrinsic distortion from planarity. In the case of **2**, this bent structure induces an angle between the C–Br bonds of *ca.* 126.5° (Scheme 1 top right. See also the Supporting Information, Table S6 and Figure S38), according to structure optimized by density functional theory (DFT) methods, which is in good agreement with the X-ray diffraction structure of a compound with the same core (see Supporting Information, Figure S41). This geometry enhances the shape complementarity with the U-shaped **3** and makes the *hept*-HBC core to suffer a reduced distortion (Scheme 1) upon incorporation into the CPP motif than planar PAHs.

Having synthesized **1**, we tackled its structural characterization. The ^{1}H NMR spectrum in $CDCl_3$ shows a set of well-defined signals at room temperature, which were assigned by means of ^{13}C and 2D NMR experiments and are in agreement with the target structure (Figure 2 and Supporting Information). Additionally, its exact mass (m/z = 1192.4591 $[M]^+$) was also identified by high-resolution matrix-assisted laser desorption ionization/time-of-flight mass spectrometry (MALDI-TOF). The isotopic distribution obtained is consistent with the calculated one, supporting the proposed structure (Supporting Information, Figures S18 and S19).

The structure of macrocycle **1** was also confirmed by single-crystal X-ray diffraction of the crystals grown by slow diffusion of acetonitrile into a solution of the compound in a mixture of $[D_4]$-1,2-dichlorobenzene and methanol.[20] In comparison with the related [10]CPP, three phenylene rings are now part of the *hept*-HBC core, which influences the geometry of the macrocycle (Scheme 1, Figure S29 and Figure 3). While [10]CPP shows in the solid state an almost circular geometry, with distances between opposite aromatic rings ranging 13.44–13.74 Å,[6b] *hept*-HBC-[10]CPP **1** displays in the crystal a more elliptical shape, with a difference of *ca.* 2 Å between the major and the minor axis (14.46 Å vs 12.48 Å) (Figure 3c). The average torsion angle between the phenylene rings and between the *hept*-HBC unit and the adjacent phenylenes is 32.6°, higher than the mean value of 27.3° exhibited by the [10]CPP.[6b] The crystal packing shows the presence of channels resulting from the alignment of the macrocycles (Figure 3a and b). We can consider that these channels are composed of subunits formed by two nanorings separated by 6.16 Å that are displaced to accommodate the *hept*-HBC cores, located towards opposite sides. These two-macrocycle subunits are then aligned in 1D with a separation of 9.11 Å, generating the tubular channels. These channels are parallelly arranged into a sort of 2D layered superstructure, however, tilted by ca. 81° (angle between [10]CPP unit mean planes) between adjacent layers (Figure 3d). In this sense, we observed the establishment of π interactions between *hept*-HBC cores of macrocycles of different layers. The shape complementarity needed for such interactions results in the hept-HBC units involved being rotated and could be one of the driving forces of the packing observed (Figure 3c).

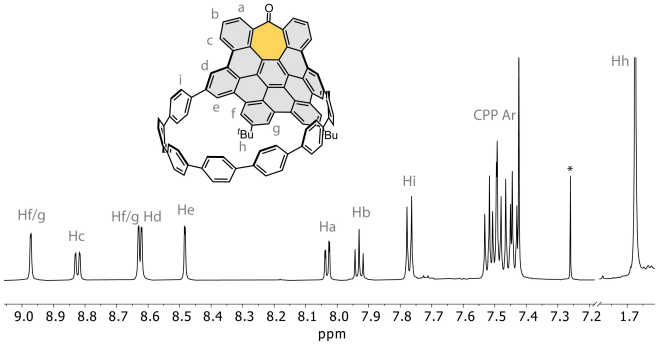

Figure 2. Partial ^{1}H NMR (600 MHz, $CDCl_3$) spectrum of *hept*-HBC [10]CPP **1**. The signal marked with the asterisk corresponds to the NMR solvent.

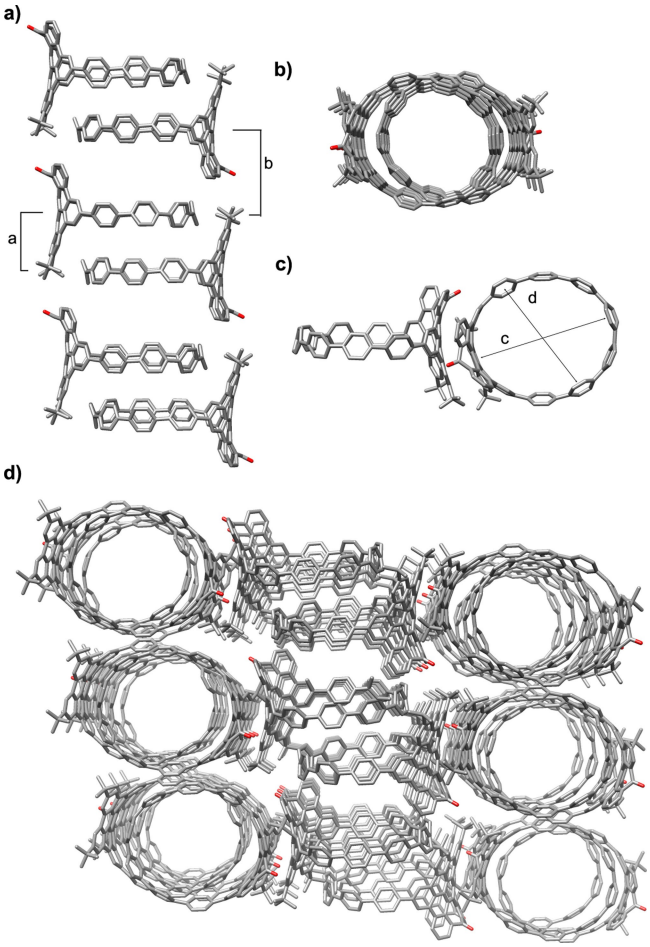

Figure 3. Crystal packing of *hept*-HBC [10]CPP **1**: a) Side and b) top views of the channels resulting from the 1D alignment of the macrocycles; c) Detail of the π interactions established between the *hept*-HBC units of different macrocycles; d) Full view of the packing showing the parallel 2D arrangement of the channels and the different orientation of the channels between layers. Distances: a) 6.16 Å; b) 9.11 Å; c) 14.46 Å; d) 12.48 Å.

The optimization by DFT calculations at the ωB97XD/def2-SVP of the structure of *hept*-HBC-[10]CPP in CH_2Cl_2 predicted a more circular geometry in solution (see the Supporting Information). From this optimized structure, we estimated the strain energy following the method applied by Itami and co-workers[21] as 48.2 kcal mol^{-1} (B3LYP/6-31G-(d)) (See Supporting Information for details), 9 kcal mol^{-1} lower than the calculated value reported for unmodified [10]CPP[21a] and much lower than the one calculated for HBC-[10]CPP.[12d] We also applied the StrainViz method[22] developed by Jasti and co-workers to estimate the local distribution of the strain within the molecule. The results (Figure S39) show that the strain in the bonds of the biphenyl systems increases when moving away from the *hept*-HBC core. Therefore, the bonds between the *hept*-HBC core and the first phenylene ring contain less strain than those on the central part of the CPP fragment. The overall strain energy estimated with this method is 48.9 kcal mol^{-1}, in good agreement with the homodesmotic approach. Both the lower value of the strain energy compared to [10]CPP and its local distribution can be attributed to the curved geometry of the *hept*-HBC derivatives (Scheme 1), which suffers a less pronounced distortion than its planar counterparts when incorporated within the cycloparaphenylene scaffold.

The optical response of **1** was investigated in toluene. The absorption spectrum of **1** features two main bands centered at 355 and 433 nm with a maximum molar extinction coefficient (ε) of 8.4×10^4 L mol^{-1} cm^{-1} (355 nm) (Figures S20 and S21), a typical value for very highly dipole-allowed electronic transitions. The experimental spectrum is in accordance with the time-dependent density functional theory (TD-DFT) calculated electronic transitions (ωB97XD/6-31++G(d,p), Supporting Information, Figure S34). When photoexciting at 400 nm, the obtained fluorescence spectrum of **1** (Figure S20) shows a structured visible band with two main peaks at 473 and 503 nm (1260 cm^{-1} spacing), related to the vibronic progression of C–C stretching modes. The emission quantum yield of macrocycle **1** has been determined as 3.7 ± 0.4 %. This compound exhibits an optical energy gap ($E_{gap,opt}$) of 2.79 eV, estimated from the crossing point of the absorption and fluorescence spectra (Figure S22).

Next, we performed cyclic and square-wave voltammetry to study the electrochemical properties of nanohoop **1**. The corresponding voltammogram in CH_2Cl_2 displays an oxidation potential at 0.79 V (vs Fc/Fc^+). However, we could not observe any clear reduction waves (Figure S27). From the onset of the first oxidation wave (Figure S28), we could estimate the energy of the HOMO (highest occupied molecular orbital) level as −5.45 eV[23] and, therefore, the LUMO (lowest unoccupied molecular orbital) lies at −2.66 eV, as estimated with the $E_{gap,opt}$ obtained from the optical measurements. From the DFT calculations (ωB97XD/6-31++G(d,p)) we could inspect the shape and distribution of those molecular orbitals. Thus, the calculations predict that the HOMO is delocalized all over the macrocycle, while the LUMO is more localized at the *hept*-HBC unit (Figure S31).

After its characterization, we moved to the study of macrocycle **1** as a supramolecular receptor for fullerenes C_{60} and C_{70}. As mentioned, [10]CPP displays a high binding affinity for fullerenes, in particular C_{60}, because of the appropriate cavity size and shape complementarity to encapsulate this curved π system. Despite the slight geometrical differences observed (see above) compared with pristine [10]CPP in the solid state, we expected that our heptagon-containing nanographene-based nanohoop **1** could also establish π-π interactions with such curved guests forming host-guest complexes, as reported earlier for HBC-[10]CPP,[12d] as the size of the fullerenes fits that of **1** predicted by theoretical calculations in solution. DFT calculations at the ωB97XD/def2-SVP theory level support this hypothesis, predicting a good size and shape complementarity between nanoring **1** and fullerenes C_{60} and C_{70}, which would enable a good fitting between them, favoring the assembly of the supramolecular complex (Figure 4 and Figures S35 and S37).

On this ground, we experimentally studied the association equilibrium. Addition of C_{60} to a solution of **1** in [D_8]-toluene results in changes in the chemical shift of the aromatic signals of the *hept*-HBC core and the cycloparaphenylene motif compatible with the binding of C_{60} within the cavity of the macrocycle (Figure S17). In parallel, we investigated the assembly of host-guest complexes by UV/Vis and photoluminescence (PL) spectroscopies with both C_{60} and C_{70}. As anticipated, macrocycle **1** displays a very marked host-guest complexation with both fullerenes, as interactions between the host and the fullerene guests are observed with both techniques. In regard to the ground electronic state, we found spectral shape modifications of the absorption band of *hept*-HBC nanoring **1** upon progressive addition of micromolar concentrations of C_{60} (Figure 5a) or C_{70} (Figure S23). These changes affect the absorption band over a very wide spectral range extending

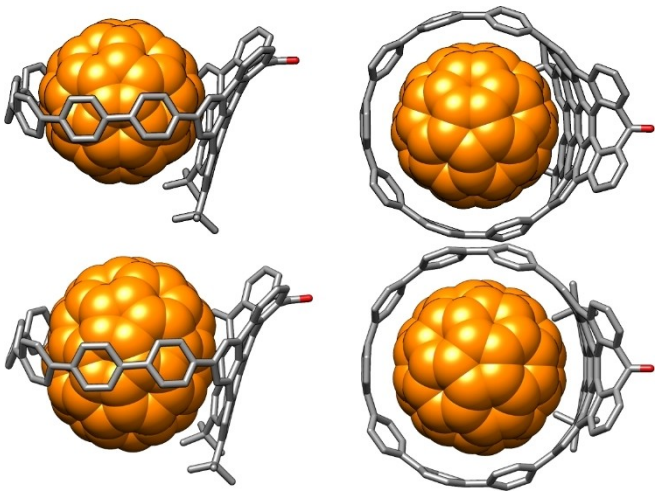

Figure 4. DFT (ωB97XD/def2-SVP) optimized structure of the host-guest complex **1**⊃C_{60} (top) and **1**⊃C_{70} (bottom). Left: side view. Right: top view. H atoms have been omitted for clarity. Color coding: C, gray (**1**) or orange (C_{60} and C_{70}); O, red.

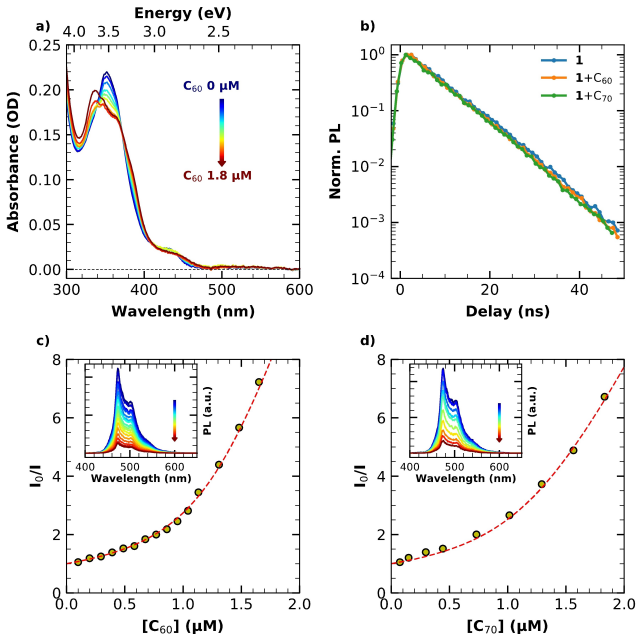

Figure 5. Top: a) UV/Vis spectra of macrocycle **1** (1×10^{-6} M) in toluene after progressive addition of C_{60} (0–1.8 μM); b) Normalized photoluminescence decay ($\lambda_{exc}=400$ nm) of macrocycle **1** (1×10^{-6} M) without guest and in the presence of C_{60} and C_{70} (1.5×10^{-6} M). Bottom: Stern–Volmer plot for the quenching of the macrocycle fluorescence upon addition of c) C_{60} and d) C_{70}. Insets: PL spectra of **1** upon addition of increasing amounts of fullerene guest.

at least from 300 to 500 nm. TD-DFT calculations (ωB97XD/6-31++G(d,p)) over the optimized inclusion complex of **1** with C_{60} (**1**⊃C_{60}, ωB97XD/def2-SVP, Figure 4) reveal that the new transitions of **1**⊃C_{60} appearing between 385 and 480 nm are dominated by charge-transfer from **1** to the C_{60} (Supporting Information, Figure S36). Therefore, considering that the LUMO energy of **1** (−2.66 eV) is higher than that of C_{60} and C_{70} (−3.7 eV),[24] we would expect the fluorescence of **1** to be quenched by the complexed fullerenes, which are very efficient electron acceptors.[24,25]

In fact, we observed that C_{60} and C_{70} strongly quench the macrocycle fluorescence with no modifications of the emission bandshape (insets of Figure 5c and d) or the emission lifetime, 6.7 ± 0.2 ns for both macrocycle **1** and its complexes (Figure 5b). The Stern–Volmer plots obtained from the fluorescence intensities recorded as a function of the concentration of C_{60} and C_{70} (Figure 5c and d) show a deviation from linearity in the quenching behavior, highlighted by an upward curvature. At the same time, the absence of lifetime changes (Figure 5b) rules out the possibility of collisional quenching, supporting that the detected quenching should occur by a non-collisional mechanism, related to the formation of host-guest complexes at the ground state level, as suggested by the absorption spectra. In fact, the nonlinear trend of the Stern–Volmer plots can be explained due to significant depletion of the fullerene concentrations upon complexation with **1**. This effect can be described by a previously reported nonlinear Stern–Volmer equation,[26] which we used to fit the titration data (see Supporting Information for more details on the fitting model). The fitting is in good agreement with the data demonstrating a 1:1 host-guest stoichiometry and allowed us to estimate the macrocycle-fullerenes binding constants as $(1.1\pm0.1)\times10^{7}$ M^{-1} for C_{60} and $(7.8\pm0.8)\times10^{6}$ M^{-1} for C_{70}. The high values obtained represent a direct indication of the strong host-guest interactions between *hept*-HBC and both C_{60} and C_{70}. Unlike our previous *hept*-HBC-based cyclophane,[16] selective for C_{70}, **1** displays a slightly higher affinity for C_{60} compared to C_{70}, which can be attributed to the well-known good size complementarity of the [10]CPP motif with C_{60}. The estimated constant for the interaction between **1** and C_{60} is of the same order of magnitude than that determined for the association of the latter with HBC-[10]CPP (2.33×10^{7} M^{-1}, toluene, UV/Vis)[12d] and almost one order of magnitude higher than the one exhibited by unmodified [10]CPP (2.79×10^{6} M^{-1}, toluene, fluorescence).[6a] In the case of the complexation of C_{70}, the increase of the thermodynamic stability of the host-guest complex assembled from **1** compared to [10]CPP is more pronounced, as the binding constant is almost three orders of magnitude higher than that reported for [10]CPP⊃C_{70} (8.4×10^{4} M^{-1}, toluene, UV/Vis).[6c] The π-extended surface of **1** in comparison with unmodified [10]CPP can explain the higher binding constants observed with fullerenes. This is especially relevant for C_{70}, as the interaction with the *hept*-HBC unit is favored by the extended π surface of the latter, able to better accommodate the shape of the C_{70} (Figure 4 bottom).

In order to obtain further information on the relaxation dynamics after photoexcitation, we carried out broadband femtosecond transient absorption (TA) measurements on **1** and on **1**⊃C_{60} and **1**⊃C_{70},[6g,27] by pumping the samples with 90 fs laser pulses at 400 nm in a femtosecond pump-probe setup.[28]

Consistently with the ns excited-state lifetime of macrocycle **1** (6.7 ± 0.2 ns), the TA signal reported in Fig. 6a shows no substantial dynamics on the sub-nanosecond time scale. As for its spectral shape, we notice the following features: (i) A negative peak around 430 nm, which closely resembles the inverted sign steady-state absorption (dash-dotted black curve). This is common in TA and can be interpreted as ground-state bleaching (GSB), that is the reduction of steady-state absorption due to the depopulation of the ground state by photoexcitation; (ii) A recognizable emission contribution, which appears in TA as stimulated emission (SE), having a similar shape as fluorescence except for a flip in sign. The SE is pinpointed by spectral features matching the main steady-state emission subpeaks (dashed green curve); (iii) All other features are due to broad excited state absorption contributions spanning over the entire spectral range.

Interestingly, the addition of C_{60} (Figure 6b, Figure S24) leads to profound spectral and dynamic changes. The shape variations of the TA signal reflect the change of both ground- and excited electronic states of **1** upon binding with C_{60}. In particular, the GSB peak redshifts from 435 (negative dip in Figure 6a) to 450 nm (negative dip in Figure 6b), as a direct consequence of the shift of steady-state absorption

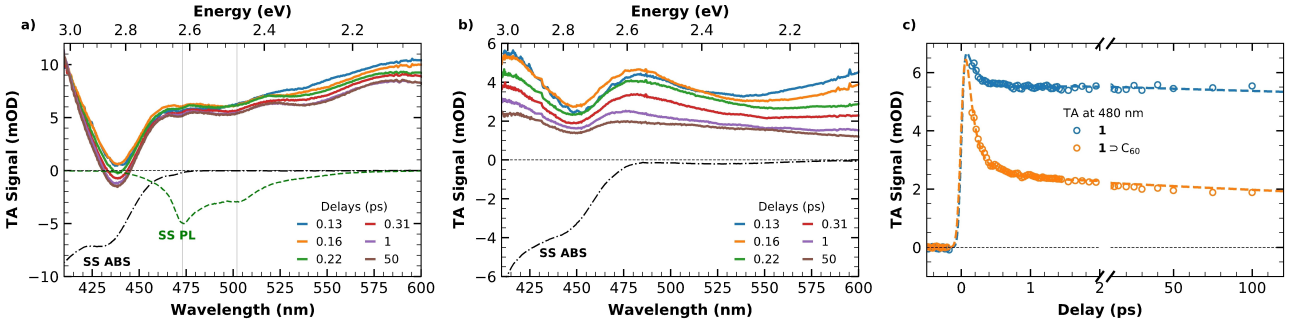

Figure 6. Transient absorption spectra acquired at different delays from photoexcitation at 400 nm of: a) Solution of macrocycle **1** in toluene (1×10^{-4} M); b) Macrocycle **1** in the presence of C_{60} (2×10^{-4} M). The signal is compared to the steady-state (SS) absorption (ABS) and photoluminescence (PL) spectra to facilitate the identification of the various contributions to the TA signal; c) Comparison of the TA signal of macrocycle **1** and complex **1**⊃C_{60} at probe wavelength of 480 nm.

features in Figure 5a. Similarly, the SE associated subpeaks disappear, as expected because of fluorescence quenching (Figure 5c). However, the most remarkable observation is that these spectral variations are already encountered at the earliest time delays accessible by our experiment, as evident when comparing the spectra at 0.13 ps in the absence (Figure 6a, blue line) and in the presence of C_{60} (Figure 6b, blue line). This result reveals that the electron transfer towards C_{60} is "instantaneous", i.e., faster than our time resolution of ≈100 fs. This conclusion agrees indeed with the emergence in **1**⊃C_{60} of new charge-transfer electronic transitions from the macrocycle to the fullerene, as predicted by the aforementioned theoretical calculations (Figure S36). In fact, the photoexcitation of such transitions should produce a direct optical charge transfer from **1** to fullerenes, which entirely occurs within the photoexcitation pulse duration leading to a quasi-instantaneous electron-hole separation.

Notably, such an ultrafast (<100 fs) charge separation is two orders of magnitude more efficient than previously reported for the host-guest complex between HBC-[10]CPP and C_{60},[12d] where electron transfer from the photoexcited macrocycle to fullerene occurred over several tens of picoseconds.

Apart from the spectral changes, also the temporal dynamics of the TA signal change from **1** to **1**⊃C_{60}. In fact, **1**⊃C_{60} displays a synchronous decay of the overall TA signal (Figure 6b), which is completely absent in **1** (Figure 6a), where the signal is essentially constant in time. Figure 6c and Figure S26 show representative kinetic traces extracted from the TA signal, together with their least-square fits with multiexponential decay functions [see Eq. (5) in the Supporting Information for details on the fitting procedure]. As can be seen in Figure 6c, evident relaxation dynamics affect the TA signal of **1**⊃C_{60} within the first ≈1 ps from photoexcitation, in contrast to isolated **1** where the TA signal is almost constant. In particular, we see that the magnitude of the **1**⊃C_{60} signal decays over the whole probed spectral range without noticeable changes of shape (Figure 6b).This decay simply indicates the progressive return of the complex back to the ground state. Thus, the initial ultrafast electron transfer in **1**⊃C_{60} is followed by a non-radiative electron-hole recombination, whose timescales were found to be τ_1 = 110 fs and τ_2 = 800 fs by a bi-exponential fit of the data in Figure 6c.

The TA data of **1**⊃C_{70} are shown in Figure S25. In this case we also observe instantaneous changes of the signal shape, which, combined with the modifications in the steady-state absorption spectra, point again to an ultra-efficient electron transfer from **1** to bound C_{70}. The absence of any SE contribution in the TA signal, as well as the results of fluorescence quenching experiments, indicate that the ground state recovery of the **1**⊃C_{70} complex still occurs through a non-radiative relaxation. However, differently from **1**⊃C_{60}, we see no obvious decay of the entire TA signal of **1**⊃C_{70} over the ps scale, as can be deducted from the comparison of Figure 6b and Figure S25. Thus, the charge separated state of **1**⊃C_{70} remarkably displays a much more long-lived character than that of **1**⊃C_{60}. This property makes **1**⊃C_{70} especially interesting for future studies as it may allow to efficiently harvest the photogenerated charges for prospective applications in photocatalysis or photovoltaics.

Conclusion

We have synthesized a new type of nanohoop based on a [10]cycloparaphenylene scaffold π-extended with a heptagon-containing HBC analog and characterized it both in solution and in the solid state. This macrocycle can act as a supramolecular receptor of fullerenes due to the π interactions established within the host cavity with those curved guests. The binding constants, estimated by fluorescence titrations, are one (with C_{60}) or two (with C_{70}) orders of magnitude higher than those reported for pristine [10]CPP.

We also studied the dynamics of the photophysical process that occur after photoexcitation by means of femtosecond transient absorption spectroscopy both for the nanohoop and its host:guest complexes. The results show an ultrafast electron transfer from macrocycle **1** to the fullerenes, several orders of magnitude faster than the one observed in a similar system incorporating the purely hexagonal HBC unit. This behavior demonstrates that dibenzocycloheptatrienone-containing HBC moieties can

act as electron-donor systems in host-guest complexes with fullerenes. While the electron transfer process is similar using both C_{60} and C_{70}, the lifetime of the charge-separated state is much higher for the latter, as no recombination is observed on the ps timescale. This response may open the door for the future application of this or related systems with such behavior in applications that take advantage of this charge-separated state, such as photocatalysis or photovoltaics. In this sense, the dibenzocycloheptatrienone motif also opens interesting possibilities for late-stage functionalization of HBC-CPPs hybrids that are currently under study.

Acknowledgements

This work has been financially supported by Junta de Andalucía-Consejería de Universidad, Investigación e Innovación and FEDER(ERDF) "A way of making Europe" (project P18-FR-2877), and grant PID2021-127521NB-I00 funded by MCIN/AEI/10.13039/501100011033 and ERDF "A way of making Europe". We thank Centro de Servicios de Informática y Redes de Comunicaciones (CSIRC), Universidad de Granada, for providing the computing time. This work made use of the infrastructure services provided by S^3IT (www.s3it.uzh.ch), the Service and Support for Science IT team at the University of Zurich. The authors would like to thank the S^3IT team for their support. Funding for open access charge: Universidad de Granada / CBUA.

Conflict of Interest

The authors declare no conflict of interest.

Data Availability Statement

The data that support the findings of this study are available in the Supporting Information of this article.

Keywords: Cycloparaphenylenes · Host-Guest Systems · Macrocycles · Nanographenes · Transient Absorption Spectroscopy

[1] S. E. Lewis, *Chem. Soc. Rev.* **2015**, *44*, 2221–2304.
[2] a) Y. Segawa, A. Yagi, K. Itami, *Phys. Sci. Rev.* **2017**, *2*, 20160102; b) M. A. Majewski, M. Stępień, *Angew. Chem. Int. Ed.* **2019**, *58*, 86–116.
[3] E. J. Leonhardt, R. Jasti, *Nat. Chem. Rev.* **2019**, *3*, 672–686.
[4] a) B. M. White, Y. Zhao, T. E. Kawashima, B. P. Branchaud, M. D. Pluth, R. Jasti, *ACS Cent. Sci.* **2018**, *4*, 1173–1178; b) S. Wang, Q. Huang, J. Wang, P. Huang, P. Fang, P. Du, *Chem. Commun.* **2021**, *57*, 11867–11870.
[5] a) D. Lu, Q. Huang, S. Wang, J. Wang, P. Huang, P. Du, *Front. Chem.* **2019**, *7*, 668; b) Y. Xu, M. von Delius, *Angew. Chem. Int. Ed.* **2020**, *59*, 559–573.
[6] a) T. Iwamoto, Y. Watanabe, T. Sadahiro, T. Haino, S. Yamago, *Angew. Chem. Int. Ed.* **2011**, *50*, 8342–8344; b) J. Xia, J. W. Bacon, R. Jasti, *Chem. Sci.* **2012**, *3*, 3018–3021; c) T. Iwamoto, Y. Watanabe, H. Takaya, T. Haino, N. Yasuda, S. Yamago, *Chem. Eur. J.* **2013**, *19*, 14061–14068; d) Y. Nakanishi, H. Omachi, S. Matsuura, Y. Miyata, R. Kitaura, Y. Segawa, K. Itami, H. Shinohara, *Angew. Chem. Int. Ed.* **2014**, *53*, 3102–3106; e) H. Ueno, T. Nishihara, Y. Segawa, K. Itami, *Angew. Chem. Int. Ed.* **2015**, *54*, 3707–3711; f) S. Hashimoto, T. Iwamoto, D. Kurachi, E. Kayahara, S. Yamago, *ChemPlusChem* **2017**, *82*, 1015–1020; g) Y. Xu, R. Kaur, B. Wang, M. B. Minameyer, S. Gsänger, B. Meyer, T. Drewello, D. M. Guldi, M. von Delius, *J. Am. Chem. Soc.* **2018**, *140*, 13413–13420; h) J. Rio, S. Beeck, G. Rotas, S. Ahles, D. Jacquemin, N. Tagmatarchis, C. Ewels, H. A. Wegner, *Angew. Chem. Int. Ed.* **2018**, *57*, 6930–6934; i) Y. Xu, B. Wang, R. Kaur, M. B. Minameyer, M. Bothe, T. Drewello, D. M. Guldi, M. von Delius, *Angew. Chem. Int. Ed.* **2018**, *57*, 11549–11553; j) X. Zhang, H. Shi, G. Zhuang, S. Wang, J. Wang, S. Yang, X. Shao, P. Du, *Angew. Chem. Int. Ed.* **2021**, *60*, 17368–17372; k) Y. Yang, S. Huangfu, S. Sato, M. Juríček, *Org. Lett.* **2021**, *23*, 7943–7948; l) Y. Yang, M. Juríček, *ChemPlusChem* **2022**, *87*, e202100468.
[7] M. Hermann, D. Wassy, B. Esser, *Angew. Chem. Int. Ed.* **2021**, *60*, 15743–15766.
[8] a) S. Hitosugi, W. Nakanishi, T. Yamasaki, H. Isobe, *Nat. Commun.* **2011**, *2*, 492; b) A. Yagi, Y. Segawa, K. Itami, *J. Am. Chem. Soc.* **2012**, *134*, 2962–2965; c) H. Isobe, S. Hitosugi, T. Yamasaki, R. Iizuka, *Chem. Sci.* **2013**, *4*, 1293–1297; d) T. Matsuno, S. Kamata, S. Hitosugi, H. Isobe, *Chem. Sci.* **2013**, *4*, 3179–3183; e) T. Iwamoto, E. Kayahara, N. Yasuda, T. Suzuki, S. Yamago, *Angew. Chem. Int. Ed.* **2014**, *53*, 6430–6434; f) A. Yagi, G. Venkataramana, Y. Segawa, K. Itami, *Chem. Commun.* **2014**, *50*, 957–959; g) M. R. Golder, C. E. Colwell, B. M. Wong, L. N. Zakharov, J. Zhen, R. Jasti, *J. Am. Chem. Soc.* **2016**, *138*, 6577–6582; h) N. Grabicki, T. D. Nguyen, S. Weidner, O. Dumele, *Angew. Chem. Int. Ed.* **2021**, *60*, 14909–14914.
[9] a) M. Ball, Y. Zhong, B. Fowler, B. Zhang, P. Li, G. Etkin, D. W. Paley, J. Decatur, A. K. Dalsania, H. Li, S. Xiao, F. Ng, M. L. Steigerwald, C. Nuckolls, *J. Am. Chem. Soc.* **2016**, *138*, 12861–12867; b) E. Kayahara, X. Zhai, S. Yamago, *Can. J. Chem.* **2017**, *95*, 351–356; c) S. Li, M. Aljhdli, H. Thakellapalli, B. Farajidizaji, Y. Zhang, N. G. Akhmedov, C. Milsmann, B. V. Popp, K. K. Wang, *Org. Lett.* **2017**, *19*, 4078–4081.
[10] Y. Kuroda, Y. Sakamoto, T. Suzuki, E. Kayahara, S. Yamago, *J. Org. Chem.* **2016**, *81*, 3356–3363.
[11] J. S. Wössner, D. Wassy, A. Weber, M. Bovenkerk, M. Hermann, M. Schmidt, B. Esser, *J. Am. Chem. Soc.* **2021**, *143*, 12244–12252.
[12] a) T. Matsuno, S. Sato, R. Iizuka, H. Isobe, *Chem. Sci.* **2015**, *6*, 909–916; b) D. Lu, G. Zhuang, H. Wu, S. Wang, S. Yang, P. Du, *Angew. Chem. Int. Ed.* **2017**, *56*, 158–162; c) S. Cui, G. Zhuang, D. Lu, Q. Huang, H. Jia, Y. Wang, S. Yang, P. Du, *Angew. Chem. Int. Ed.* **2018**, *57*, 9330–9335; d) Q. Huang, G. Zhuang, H. Jia, M. Qian, S. Cui, S. Yang, P. Du, *Angew. Chem. Int. Ed.* **2019**, *58*, 6244–6249; e) S. Wang, X. Li, G. Zhuang, M. Chen, P. Huang, S. Yang, P. Du, *Chem. Commun.* **2021**, *57*, 9104–9107; f) J. Wang, X. Zhang, H. Jia, S. Wang, P. Du, *Acc. Chem. Res.* **2021**, *54*, 4178–4190; g) S. Wang, X. Li, K. Wei, X. Zhang, S. Yang, G. Zhuang, P. Du, *Eur. J. Org. Chem.* **2022**, e202101493.
[13] a) M. Quernheim, F. E. Golling, W. Zhang, M. Wagner, H.-J. Räder, T. Nishiuchi, K. Müllen, *Angew. Chem. Int. Ed.* **2015**, *54*, 10341–10346; b) D. Lu, H. Wu, Y. Dai, H. Shi, X. Shao, S. Yang, J. Yang, P. Du, *Chem. Commun.* **2016**, *52*, 7164–7167; c) Y. Nakagawa, R. Sekiguchi, J. Kawakami, S. Ito, *Org. Biomol. Chem.* **2019**, *17*, 6843–6853; d) H. Jia, G. Zhuang, Q. Huang, J. Wang, Y. Wu, S. Cui, S. Yang, P. Du, *Chem. Eur. J.* **2020**, *26*, 2159–2163.

[14] For selected examples, see: a) A. Sygula, F. R. Fronczek, R. Sygula, P. W. R., M. M. Olmstead, *J. Am. Chem. Soc.* **2007**, *129*, 3842–3843; b) D.-C. Yang, M. Li, C.-F. Chen, *Chem. Commun.* **2017**, *53*, 9336–9339; c) M. Takeda, S. Hiroto, H. Yokoi, S. Lee, D. Kim, H. Shinokubo, *J. Am. Chem. Soc.* **2018**, *140*, 6336–6342; d) A. Sacristán-Martín, H. Barbero, S. Ferrero, D. Miguel, R. García-Rodríguez, C. M. Álvarez, *Chem. Commun.* **2021**, *57*, 11013–11016.

[15] a) Z. Wang, F. Dötz, V. Enkelmann, K. Müllen, *Angew. Chem. Int. Ed.* **2005**, *44*, 1247–1250; b) N. J. Tremblay, A. A. Gorodetsky, M. P. Cox, T. Schiros, B. Kim, R. Steiner, Z. Bullard, A. Sattler, W.-Y. So, Y. Itoh, M. F. Toney, H. Ogasawara, A. P. Ramirez, I. Kymissis, M. L. Steigerwald, C. Nuckolls, *ChemPhysChem* **2010**, *11*, 799–803; c) S. J. Kang, J. B. Kim, C.-Y. Chiu, S. Ahn, T. Schiros, S. S. Lee, K. G. Yager, M. F. Toney, Y.-L. Loo, C. Nuckolls, *Angew. Chem. Int. Ed.* **2012**, *51*, 8594–8597; d) X. Gu, H. Li, B. Shan, Z. Liu, Q. Miao, *Org. Lett.* **2017**, *19*, 2246–2249; e) A. H. G. David, S. Míguez-Lago, C. M. Cruz, J. M. Cuerva, V. Blanco, A. G. Campaña, *Org. Mater.* **2021**, *3*, 51–59; f) S. Zank, J. M. Fernández-García, A. J. Stasyuk, A. A. Voityuk, M. Krug, M. Solà, D. M. Guldi, N. Martín, *Angew. Chem. Int. Ed.* **2022**, *61*, e202112834.

[16] V. G. Jiménez, A. H. G. David, J. M. Cuerva, V. Blanco, A. G. Campaña, *Angew. Chem. Int. Ed.* **2020**, *59*, 15124–15128.

[17] S. Castro-Fernández, C. M. Cruz, I. F. A. Mariz, I. R. Márquez, V. G. Jiménez, L. Palomino-Ruiz, J. M. Cuerva, E. Maçôas, A. G. Campaña, *Angew. Chem. Int. Ed.* **2020**, *59*, 7139–7145.

[18] I. R. Márquez, N. Fuentes, C. M. Cruz, V. Puente-Muñoz, L. Sotorrios, M. L. Marcos, D. Choquesillo-Lazarte, B. Biel, L. Crovetto, E. Gómez-Bengoa, M. T. González, R. Martin, J. M. Cuerva, A. G. Campaña, *Chem. Sci.* **2017**, *8*, 1068–1074.

[19] R. Jasti, J. Bhattacharjee, J. B. Neaton, C. R. Bertozzi, *J. Am. Chem. Soc.* **2008**, *130*, 17646–17647.

[20] Deposition Number 2237075 (for **1**) contains the supplementary crystallographic data for this paper. These data are provided free of charge by the joint Cambridge Crystallographic Data Centre and Fachinformationszentrum Karlsruhe Access Structures service.

[21] a) Method used: Y. Segawa, H. Omachi, K. Itami, *Org. Lett.* **2010**, *12*, 2262–2265; b) For the group equivalent reaction, see: S. M. Bachrach, *J. Chem. Educ.* **1990**, *67*, 907–908.

[22] C. E. Colwell, T. W. Price, T. Stauch, R. Jasti, *Chem. Sci.* **2020**, *11*, 3923–3930.

[23] J. Pommerehne, H. Vestweber, W. Guss, R. F. Mahrt, H. Bässler, M. Porsch, J. Daub, *Adv. Mater.* **1995**, *7*, 551–554.

[24] H.-S. Lin, I. Jeon, R. Xiang, S. Seo, J.-W. Lee, C. Li, A. Pal, S. Manzhos, M. S. Goorsky, Y. Yang, S. Maruyama, Y. Matsuo, *ACS Appl. Mater. Interfaces* **2018**, *10*, 39590–39598.

[25] a) N. Martín, L. Sánchez, B. Illescas, I. Pérez, *Chem. Rev.* **1998**, *98*, 2527–2547; b) A. V. Baskar, M. R. Benzigar, S. N. Talapaneni, G. Singh, A. S. Karakoti, J. Yi, A. H. Al-Muhtaseb, K. Ariga, P. M. Ajayan, A. Vinu, *Adv. Funct. Mater.* **2022**, *32*, 2106924.

[26] K. Campbell, A. Zappas, U. Bunz, Y. S. Thio, D. G. Bucknall, *J. Photochem. Photobiol. A* **2012**, *249*, 41–46.

[27] F. Schwer, S. Zank, M. Freiberger, R. Kaur, S. Frühwald, C. C. Robertson, A. Görling, T. Drewello, D. M. Guldi, M. von Delius, *Org. Mater.* **2022**, *4*, 7–17.

[28] A. Sciortino, F. Ferrante, G. Gonçalves, G. Tobias, R. Popescu, D. Gerthsen, N. Mauro, G. Giammona, G. Buscarino, F. M. Gelardi, S. Agnello, M. Cannas, D. Duca, F. Messina, *ACS Appl. Mater. Interfaces* **2021**, *13*, 49232–49241.

Manuscript received: January 27, 2023
Accepted manuscript online: March 21, 2023
Version of record online: April 18, 2023